THE NEUTRON-NEUTRON S-STATE INTERACTION

V. K. VOĬTOVETSKIĬ, I. L. KORSUNSKIĬ, and Yu. F. PAZHIN

Submitted to JETP editor March 4, 1964

J. Exptl. Theoret. Phys. (U.S.S.R.) 47, 1612-1627 (November, 1964)

The proton spectrum near the upper limit for the D(n, p)2n reaction is investigated to determine the neutron-neutron scattering length a_{nn}. A scintillation spectrometer that completely separates deuterons from protons is employed. The spectrum is described using an expression for the differential cross section of the reaction, obtained by analyzing the nonrelativistic Feynman diagrams corresponding to nucleon-deuteron inelastic scattering. The neutron-neutron scattering length and the singlet state energy are derived by comparing the experimental spectrum with the theoretical dependence of the differential cross section on proton energy; the respective values are $a_{nn} = -23.6^{-1.6}_{+2.0}$ F and $\epsilon_{nn} = 67^{+12}_{-9}$ keV.

FOR the direct verification of charge independence in the S state the neutron-proton and neutron-neutron forces must be compared at low energies. The parameters of the neutron-proton singlet state have been measured very accurately in scattering experiments.[1] To determine the strength of the forces between neutrons one can similarly investigate reactions in which two neutrons are produced with small relative momentum $\hbar\mathbf{f}$.

Migdal [2] and Watson [3] have shown that the energy distribution of particles with small values of $\mathbf{f}$ is greatly affected by their interaction in the final state; the amplitude of the inelastic process in which these particles are produced is proportional to the amplitude of the scattering of one particle by the other. This result is universal and is used widely in investigating the interactions of unstable particles.

Experiments on elementary reactions offer the advantage that difficulties associated with the branch involving an intermediate nucleus are obviated. In the well-known experiments of Panofsky et al [4] and of Phillips and Crowe,[5] who obtained the first direct information regarding the character of the neutron-neutron forces, the capture of a π^- meson by deuterium was investigated.

For the study of the neutron-neutron interaction a suitable reaction is D(n, p)2n, where the attraction between the neutrons influences the shape of the proton energy spectrum. The scattering length a_{nn} (and the singlet state energy ϵ_{nn}) can be determined by comparing, in the region of small $\mathbf{f}$, the experimental spectrum with the theoretical spectrum containing a parameter characterizing the interaction.

For small values of f the c.m.s. differential cross section for the reaction is

$$d\sigma = \frac{b}{f^2 + 1/a_{nn}^2}\rho(\mathbf{f}, \mathbf{k}')\,df\,d\mathbf{k}' = \frac{b_1(E_{p'}^m - E_{p'})^{1/2}\sqrt{E_{p'}}}{E_{p'}^m - E_{p'} + {}^2/_3\varepsilon_{nn}}\,dE_{p'}\,d\Omega_{p'}. \quad (1)$$

Here $[f^2 + a_{nn}^{-2}]^{-1}$ is the resonance factor for interaction of the neutrons in the final state, $\hbar\mathbf{k}'$ is the proton momentum, $\rho(\mathbf{f}, \mathbf{k}')\,df d\mathbf{k}'$ is the statistical weight of the final states, b and b_1 contain the contribution from the nucleon interaction during the reaction process, E_p' is the proton energy, $E_p'^m$ is the maximum value of E_p', and $d\Omega_p'$ is the solid angle within which protons are emitted.

Equation (1) shows that the energy distribution possesses a maximum. At the spectral edge, where the momentum $\hbar\mathbf{f}$ is very small, it can be assumed that b_1 is constant in (1). In this approximation the distance of the maximum from the upper limit of the spectrum is [1)]

$$d = {}^2/_3\varepsilon_{nn}(1 - 4\,\varepsilon_{nn}/3E_{p'}^m).$$

The sensitivity of the spectral shape to ϵ_{nn} can be judged from the relationship between ϵ_{nn} and l_n, the width of the peak at 1/n of maximum. For a rough estimate with $n \leq 1.5$ we assume that in (1) the quantity b_1 also remains constant in this broader region of the spectrum; then

$$l_n \approx {}^8/_3n\varepsilon_{nn}. \quad (2)$$

To determine ϵ_{nn} we must derive the exact theoretical dependence of $d^2\sigma/dE_p'd\Omega_p'$ on E_p' and measure the proton spectrum at its upper limit.

[1)] It is extremely difficult to measure d very accurately in the reaction D(n,p)2n.

In the present work we have investigated the proton spectrum from 7.5 to 12 MeV and have obtained ϵ_{nn}.

1. THEORETICAL SHAPE OF PROTON SPECTRUM AT ITS UPPER LIMIT

In (1) the dependence on f is given explicitly only for the interaction in the final state. To determine the exact shape of the spectrum we must consider the entire process in which a neutron is scattered inelastically by a deuteron. Skornyakov and Ter-Martirosyan [6] derived an equation for the wave function of a three-particle system with short-range resonance forces in the zeroth approximation ($r_0 \to 0$, r_0 being the range of the force). This equation was investigated by Danilov,[7] who proposed a means of eliminating the ambiguity in the solution for the state with $S = 1/2$. Danilov also obtained the equation in a linear approximation with respect to a parameter proportional to r_0.[8]

Results agreeing with experiment were obtained [9] when the amplitude for the elastic scattering of a zero-energy neutron by a deuteron was calculated by Danilov's method.[7] However, this method of solving the equation is extremely complicated in the general case of inelastic scattering. It has been shown by a number of authors that nuclear reactions can be described by nonrelativistic Feynman diagrams. Direct processes have been studied using the diagram method.[10-12] It follows from [10] that the Butler theory of stripping can be represented by a pole diagram. In [11,12] Shapiro showed the importance of more complicated diagrams (triangular etc.) for the theory of direct processes, as well as the possibility of utilizing the diagram method to consider the interaction in the initial and final states.

Komarov and Popova [12] summed an infinite series of nonrelativistic perturbation-theory diagrams representing a reaction involving three nucleons on the assumption of two-particle interactions. They derived an equation for the wave function of the system which coincides with the Skornyakov-Ter-Martirosyan equation in the zeroth approximation with respect to the reaction radius, while in the linear approximation it coincides with Danilov's equation. If in describing the proton spectrum for the reaction D(n, p)2n we confine ourselves to energies associated with relatively small f, the differential cross section containing one experimentally determinable constant (besides ϵ_{nn}) can be derived directly from an analysis of the set of diagrams corresponding to the process. All possible reactions in which a deuteron is split by a nucleon can be represented by the following sum of diagrams:[13]

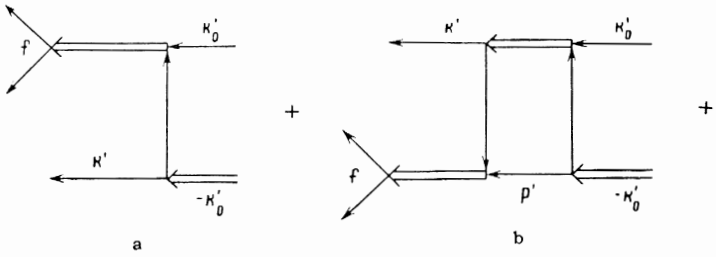

In this sum each diagram includes three graphs of a single type which differ by an interchange of the particles in the final state.

For the reaction D(n, p)2n the entire series of diagrams contains two groups corresponding, respectively, to the final-state interaction of two neutrons and of a neutron and proton. The total amplitude for the first group of diagrams is [2)]

$$A^{nn}(\mathbf{k}', \mathbf{k}_0') = A_1^{nn}(\mathbf{k}', \mathbf{k}_0') + A_2^{nn}(\mathbf{k}', \mathbf{k}_0') + A_n^{nn}(\mathbf{k}', \mathbf{k}_0'), \tag{3}$$

where $A_1^{nn}(\mathbf{k}', \mathbf{k}_0')$ is the contribution from the pole diagram a, $A_2^{nn}(\mathbf{k}', \mathbf{k}_0')$ is the contribution from the square diagram b, $A_n^{nn}(\mathbf{k}', \mathbf{k}_0')$ is the contribution from all other diagrams, $\hbar\mathbf{k}_0$ is the incident-neutron momentum, and $\hbar\mathbf{k}'$ is the c.m.s. proton momentum following inelastic scattering.

In the linear approximation with respect to r_0 we have

$$A_1^{nn}(\mathbf{k}', \mathbf{k}_0') = \varkappa\gamma(f)\frac{1}{\alpha_t^2 + (\mathbf{k}' + \mathbf{k}_0'/2)^2} = \varkappa\gamma(f)\frac{1}{\alpha_t^2 + k^2}; \tag{4}$$

where

$$\varkappa = \frac{8\pi(3\pi\alpha_t)^{1/2}}{m(1 - {}^1/_2\alpha_t r_{0t})}, \quad \gamma(f) = \frac{1}{a_{nn} + if - {}^1/_2 r_{0s}(a_{nn}^2 + f^2)},$$

m is the nucleon mass, $\alpha_t = 1/a_t$, $\alpha_{nn} = 1/a_{nn}$, a_t is the triplet n-p scattering length, r_{0t} is the triplet effective radius, r_{0s} is the singlet effective radius, and $\hbar\mathbf{k}$ is the laboratory-system proton momentum after scattering.

The pole diagram corresponds to the Chew and Low approximation [14] and to the first iteration of the Skornyakov-Ter-Martirosyan (for $r_0 \to 0$) and Danilov equations. This diagram makes a considerable contribution to the region of the proton spectrum where $\hbar\mathbf{k}$ is small.

In the contribution of the square diagram to the amplitude $A_2^{nn}(\mathbf{k}', \mathbf{k}_0')$ following integration over

[2)] Coefficients representing functions of spin and isospin variables are included in the expressions for the amplitudes.

energy we can distinguish a part containing an important dependence on f even in the primary interaction:

$$A_2^{nn}(\mathbf{k}', \mathbf{k}_0') = \frac{1}{4}\varkappa\gamma(f)\left\{\left[-\frac{1}{\alpha_t + if_1' - {}^1/_2 r_{0t}(\alpha_t^2 + f_1'^2)}\right.\right.$$
$$-\frac{1}{\alpha_s + if_1' - {}^1/_2 r_{0s}(\alpha_s^2 + f_1'^2)}$$
$$-\frac{1}{\alpha_t + if_2' - {}^1/_2 r_{0t}(\alpha_t^2 + f_2'^2)}$$
$$\left.-\frac{1}{\alpha_s + if_2' - {}^1/_2 r_{0s}(\alpha_s^2 + f_2'^2)}\right]$$
$$\times \int \frac{1}{\alpha_t^2 + (\mathbf{p}' + \mathbf{k}_0'/2)^2}\frac{d\mathbf{p}'}{-f^2 + (\mathbf{p}' + \mathbf{k}'/2)^2}$$
$$\left.+ B_2^{nn}(\mathbf{k}', \mathbf{k}_0')\right\} = \frac{1}{4}\varkappa\gamma(f)$$
$$\times\left\{\left[-\frac{1}{\alpha_t + if_1' - {}^1/_2 r_{0t}(\alpha_t^2 + f_1'^2)}\right.\right.$$
$$-\frac{1}{\alpha_s + if_1' - {}^1/_2 r_{0s}(\alpha_s^2 + f_1'^2)}$$
$$-\frac{1}{\alpha_t + if_2' - {}^1/_2 r_{0t}(\alpha_t^2 + f_2'^2)}$$
$$\left.-\frac{1}{\alpha_s + if_2' - {}^1/_2 r_{0s}(\alpha_s^2 + f_2'^2)}\right]$$
$$\times\frac{1}{2iq}\ln\frac{\alpha_t - i(f-q)}{\alpha_t - i(f+q)} + B_2^{nn}(\mathbf{k}', \mathbf{k}_0')\Big\}, \tag{5}$$

where $\alpha_S = 1/a_S$, $\mathbf{q} = (\mathbf{k}_0' - \mathbf{k}')/2$, a_S is the singlet length of n-p scattering, $\hbar\mathbf{p}'$ is the neutron momentum in the intermediate state, and $\hbar\mathbf{f}_1'$, $\hbar\mathbf{f}_2'$ are the momenta of relative motion of the nucleons participating in the primary interaction with $\mathbf{p}' + \mathbf{k}'/2 \sim \mathbf{f}$.

If we neglect multiple scattering in the interaction of the proton with an incident neutron, the square diagram becomes triangular with the amplitude [3)]

$$A_{02}^{nn}(\mathbf{k}', \mathbf{k}_0') = \frac{1}{2}\varkappa\gamma(f)\frac{r_{0s} + r_{0t}}{2}\frac{1}{2iq}\ln\frac{\alpha_t - i(f-q)}{\alpha_t - i(f+q)}. \tag{6}$$

Combinations of a pole diagram and a triangular diagram correspond to matrix elements for the Born approximation taking account of interaction in the final state.[13]

For the second group of diagrams the total amplitude is

$$A^{np}\left(\mathbf{f} - \frac{1}{2}\mathbf{k}', \mathbf{k}_0'\right) + A^{np}\left(-\mathbf{f} - \frac{1}{2}\mathbf{k}', \mathbf{k}_0'\right)$$
$$= A_1^{np}\left(\mathbf{f} - \frac{1}{2}\mathbf{k}', \mathbf{k}_0'\right) + A_2^{np}\left(\mathbf{f} - \frac{1}{2}\mathbf{k}', \mathbf{k}_0'\right)$$
$$+ A_n^{np}\left(\mathbf{f} - \frac{1}{2}\mathbf{k}', \mathbf{k}_0'\right) + A_1^{np}\left(-\mathbf{f} - \frac{1}{2}\mathbf{k}', \mathbf{k}_0'\right)$$
$$+ A_2^{np}\left(-\mathbf{f} - \frac{1}{2}\mathbf{k}', \mathbf{k}_0'\right) + A_n^{np}\left(-\mathbf{f} - \frac{1}{2}\mathbf{k}', \mathbf{k}_0'\right). \tag{7}$$

The contribution of the pole diagrams is

$$A_1^{np}\left(\mathbf{f} - \frac{1}{2}\mathbf{k}', \mathbf{k}_0'\right) + A_1^{np}\left(-\mathbf{f} - \frac{1}{2}\mathbf{k}', \mathbf{k}_0'\right)$$
$$= \frac{1}{4}\varkappa\left\{\left[\frac{1}{\alpha_t + if_1 - {}^1/_2 r_{0t}(\alpha_t^2 + f_1^2)}\right.\right.$$
$$\left.+\frac{1}{\alpha_s + if_1 - {}^1/_2 r_{0s}(\alpha_s^2 + f_1^2)}\right]$$
$$\times\frac{1}{\alpha_t^2 + (\mathbf{f} - \mathbf{k}'/2 + \mathbf{k}_0'/2)^2} + \left[\frac{1}{\alpha_t + if_2 - {}^1/_2 r_{0t}(\alpha_t^2 + f_2^2)}\right.$$
$$\left.\left.+\frac{1}{\alpha_s + if_2 - {}^1/_2 r_{0s}(\alpha_s^2 + f_2^2)}\right]\frac{1}{\alpha_t^2 + (-\mathbf{f} - \mathbf{k}'/2 + \mathbf{k}_0'/2)^2}\right\}, \tag{8}$$

where $\hbar\mathbf{f}_1$ and $\hbar\mathbf{f}_2$ are the momenta of relative motion of the neutron and proton, respectively, in the final state.

When protons are detected at small angles we have $q^2/(a_t^2 + f^2) \ll 1$. In this case

$$A_2^{nn}(\mathbf{k}', \mathbf{k}_0') \to A_2'^{nn}(\mathbf{k}', \mathbf{k}_0')$$
$$= \frac{1}{2}\varkappa\gamma(f)\left\{\left[-\frac{1}{\alpha_t + ik/2 - {}^1/_2 r_{0t}(\alpha_t^2 + k^2/4)}\right.\right.$$
$$\left.-\frac{1}{\alpha_s + ik/2 - {}^1/_2 r_{0s}(\alpha_s^2 + k^2/4)}\right]$$
$$\times\frac{\alpha_t + if}{\alpha_t^2 + f^2} + B_2'^{nn}(\mathbf{k}', \mathbf{k}_0')\Big\}, \tag{9}$$

$$A_1^{np}\left(\mathbf{f} - \frac{1}{2}\mathbf{k}, \mathbf{k}_0'\right) + A_1^{np}\left(-\mathbf{f} - \frac{1}{2}\mathbf{k}', \mathbf{k}_0'\right)$$
$$\to A_1'^{np}\left(\mathbf{f} - \frac{1}{2}\mathbf{k}', \mathbf{k}_0'\right) + A_1'^{np}\left(-\mathbf{f} - \frac{1}{2}\mathbf{k}', \mathbf{k}_0'\right)$$
$$= \frac{1}{2}\varkappa\left[\frac{1}{\alpha_t + ik/2 - {}^1/_2 r_{0t}(\alpha_t^2 + k^2/4)}\right.$$
$$\left.+\frac{1}{\alpha_s + ik/2 + {}^1/_2 r_{0s}(\alpha_s^2 + k^2/4)}\right]\frac{1}{\alpha_t^2 + f^2}. \tag{10}$$

Gribov has shown [16,17] that for small f the total amplitude of a reaction producing three particles must be

[3)] The contribution of the triangular diagram to the amplitude was calculated for the general case by determining singularities in [15].

$$A(\mathbf{k}', \mathbf{f}, \mathbf{k}_0') = \gamma(f) B(\mathbf{k}', \mathbf{f}, \mathbf{k}_0'), \qquad (11)$$

where $B(\mathbf{k}', \mathbf{f}, \mathbf{k}_0')$ is constant up to quadratic terms in f.

The linear dependence of $A_2'^{nn}$ on f is compensated by the contribution to $B(\mathbf{k}', \mathbf{f}, \mathbf{k}_0')$ from pole diagrams corresponding to the neutron-proton interaction in the final state.

Neglecting terms $\sim f^2/k_0'^2$, the contribution to $B(\mathbf{k}', \mathbf{f}, \mathbf{k}_0')$ from square diagrams [except for the explicit factor in $A_2'^{nn}(\mathbf{k}', \mathbf{k}_0')$] and more complicated diagrams containing a large number of interior lines can be represented by the complex constant C + iD, which is determined by the normalization; in the expression for the differential cross section normalized to the experimental spectrum, the contribution is approximated accurately by the constant iD', with $D' = \xi(C, D)$.

When we take into account the density of final states, integrate over the solid angle containing all directions of f, and introduce other numerical coefficients, the differential cross section for the reaction (when protons are detected at small angles) is

$$d\sigma = \frac{2}{\pi} \frac{\alpha_t}{1 - r_{0t}\alpha_t} \frac{1 + r_{0s}a_{nn}}{a_{nn}^2 + f^2} \left| \frac{1}{\alpha_t^2 + k^2} - \frac{1}{2}\left[\frac{1}{\alpha_t + ik/2 - {}^1/_2 r_{0t}(\alpha_t^2 + k^2/4)} + \frac{1}{\alpha_s + ik/2 - {}^1/_2 r_{0s}(\alpha_s^2 + k^2/4)} \right] \times \frac{\alpha_t - a_{nn} + {}^1/_2 r_{0s}(a_{nn}^2 + f^2)}{\alpha_t^2 + f^2} + iD' \right|^2 \frac{kf}{k_0} k dk d\Omega_p. \qquad (12)$$

Here $\hbar\mathbf{k}_0$ is the incident neutron momentum and Ω_p is the solid angle within which protons are emitted (both in the laboratory system).

2. EXPERIMENTAL PROCEDURE

The experimental investigation of the proton spectrum in the reaction D(n, p)2n[4] is considerably complicated by elastic scattering, for which the cross section is 20 times greater than the cross section for the production of protons with near-maximum energies. The absolute magnitude of the differential cross section for the inelastic process is also small.

Figure 1 shows the spectrum of particles emitted at 0° in the interaction of fast neutrons

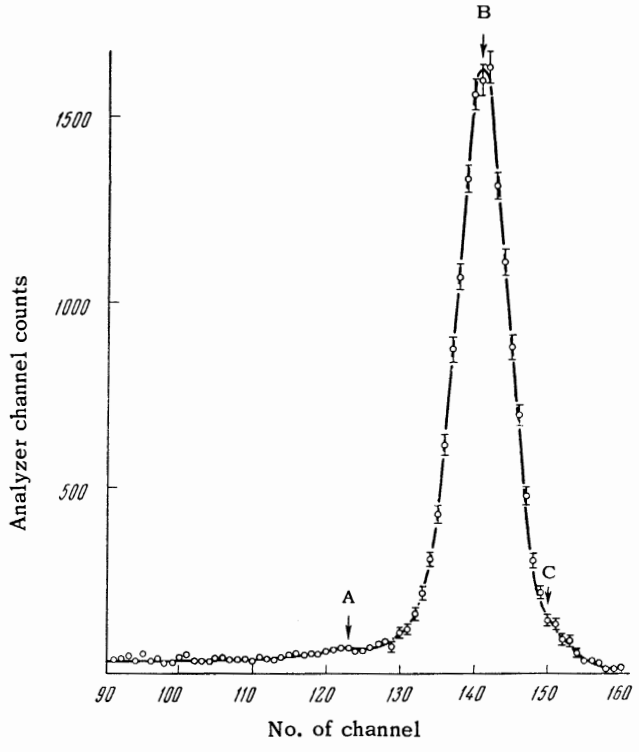

FIG. 1. Pulse-height distribution for particles emitted at 0° in the interaction of fast neutrons (13.9 MeV) with deuterium nuclei. A – position of peak in spectrum of protons produced in inelastic neutron scattering by deuterium; B – recoil deuterons; C – position of recoil proton peak. In the proton energy scale the deuteron peak is shifted toward higher energies because a CsI(Tl) crystal has unequal luminescence yields for deuterons and protons ($S_D/S_P \approx 1.05$).

with deuterium nuclei. The peak at the upper limit of the proton spectrum, which is associated with the neutron-neutron interaction in the final state, is completely masked by the strong recoil-deuteron line. Therefore, to measure the proton energy distribution we require a spectrometer with highly stable amplification during prolonged measurements, and capable of discriminating the different particle masses. In the present work we used a scintillation spectrometer which completely separated the protons from the deuterons.[19]

The experimental setup is represented in Fig. 2. Neutrons having the energy 13.9 MeV (with a spread of less than 1%), which were produced in the interaction of accelerated deuterium ions with tritium nuclei, caused the splitting of deuterons in deuterated polyethylene film. Protons emitted at 0° were analyzed by the scintillation spectrometer, a "telescope" consisting of three counters in conjunction with CsI(Tl) crystals. The deuterium radiator and scintillation counters were located in an evacuated vessel. Thin crystals

[4] The proton spectrum in the reaction D(n,p)2n has also been investigated in[18] and elsewhere.

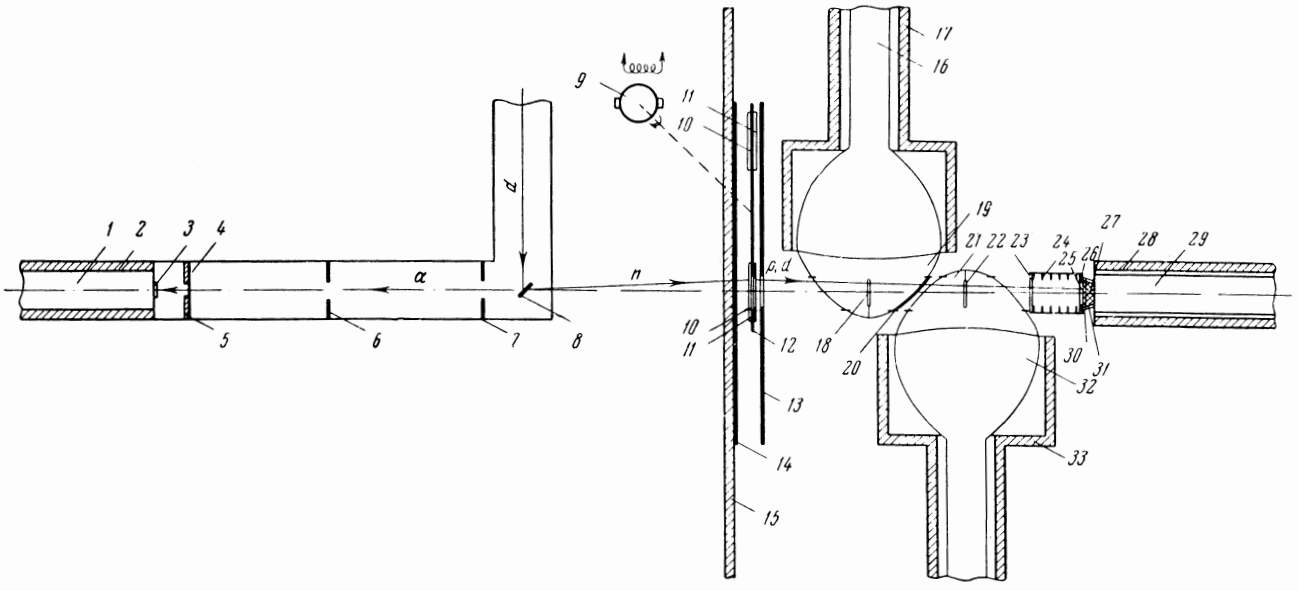

FIG. 2. Experimental arrangement. 1 – scintillation detector of α particles (neutron flux monitor); 2, 17, 28, 33 – Permalloy shields; 3, 18, 22, 30 – CsI(Tl) crystals; 4, 6, 7, 24 – anti-scattering diaphragms; 5 – graphite shield; 8 – tritium target; 9 – target exchange mechanism; 10 – target-radiator; 11, 26 – tantalum limiting rings; 12 – disk holding radiators; 13, 14 – lead shields; 15 – front wall of evacuated vessel; 16, 29, 32 – photomultipliers; 19, 21 – parabolic reflectors; 20, 23 – aluminized organic films; 25, 31 – reflectors; 27 – light pipe.

(80 and 160 μ) were used in the first and second counters, and paraboloidal aluminum reflectors were used to collect light; the crystal of the third counter was 1.8 mm thick. Protons lost about 15% of their energy in the crystals of the first two counters. To separate the protons from deuterons having identical total energies we used their different total energy losses in the first two scintillators.

In the Landau-Symon theory [20,21] the shapes of the statistical distribution curves of energy losses depend on the ratio between the quantities Δ and E_m; Δ is the width of the loss distribution curve, and E_m is the maximum energy loss in a single collision. When the condition $\Delta \gg E$ is not fulfilled the loss distributions are asymmetric and overlap for protons and deuterons of equal energies, despite a considerable difference between their mean losses.

For $\Delta \gg E_m$ the relative statistical spread of the energy losses is considerably reduced, and the loss distribution functions become Gaussian functions which do not overlap for deuterons and protons in the same very narrow energy range. The criterion for this last condition is the size of the parameter $G = 2Cm_e c^2 x/\beta^2 E_m$, where m_e is the electron mass, c is the velocity of light, β is the incident-particle velocity in units of light velocity, x is the thickness of matter in g/cm^2, C is a constant for the given absorber; $\Delta \gg E_m$ if $G \gg 1$. In telescopes with proportional counters for loss measurements we have $G < 1$.

The losses in the first two counters of the scintillation telescope were relatively large; this corresponds to the condition $G > 1$ with nonoverlapping distributions that closely resemble Gaussian functions. Thus in the scintillation telescope for protons and deuterons we have a unique correspondence between the energy and the interval of energy losses in the first two scintillators. This provides a criterion for distinguishing the deuteron and proton components in the total energy spectrum of registered emitted particles.

The energy loss spectra are determined using the amplitude distribution of the pulse sum from the first two scintillation counters; the total energy spectra are determined by the pulse-height analysis of the combined pulses from all the counters of the telescope. We used a two-dimensional analyzing setup with 300 channels for analyzing the total energy and 100 channels for analyzing the loss. The analysis was controlled by triple coincidences of pulses from the counters.

The spectrometer resolution was determined from the peak of recoil protons emitted at 0° when 13.9-MeV neutrons were scattered; the half-width of the peak was 5.5%.

The position of the analogous peak for recoil protons produced when neutrons were scattered

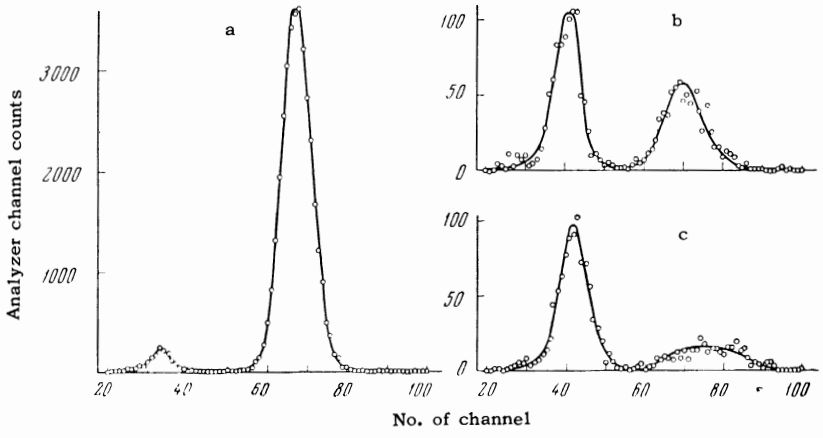

FIG. 3. Spectra of combined energy losses in the first two crystals of the spectrometer by particles emitted in neutron scattering on deuterium. Energy ranges: a) 11.65 – 14.0 MeV; b) 10.7 – 11.65 MeV; c) 9.8 – 10.7 MeV.

by residual hydrogen in a deuterated polyethylene radiator was used to monitor the stability of the spectrometer amplification during the measurements. The overall stability during prolonged measurements was 0.2%. The absolute yield was determined and the neutron intensity was monitored by registration, with fixed geometry (with a precisely determined solid angle), of α particles emitted in the reaction $T(d, n)He^4$.

3. EXPERIMENTAL RESULTS

Figure 3 shows the measured distributions of the combined energy losses in the first two crystals for the particles emitted in the neutron-deuterium interaction. These distributions pertain to the energy ranges: a) 11.65—14.0 MeV, b) 10.7—11.65 MeV, and c) 9.8—10.7 MeV. The mean energy loss is $\Delta E_m \geq 2$. These losses correspond to $G \geq 6.6$, and we observe that the energy loss regions for protons and for deuterons are completely separated in the figure.

In obtaining the selective energy spectra we analyzed simultaneously the total energy and energy loss. We registered only the events exhibiting a characteristic correspondence between the analyzed quantities for the selected type of particle.

Figure 4 shows the proton energy distribution obtained under the aforesaid conditions from the reaction $D(n, p)2n$; the protons were emitted from a radiator 4.3 mg/cm^2 thick. The measurements were obtained at the angle 0° (the mean angle ϑ_0 of proton emission with respect to the neutron flux direction was 4.5°). The spectrometer energy scale was based on the position of the recoil proton peak and was refined by comparing the experimental spectrum with the calculated distributions.

The background measured without a radiator was first subtracted from the proton spectrum.

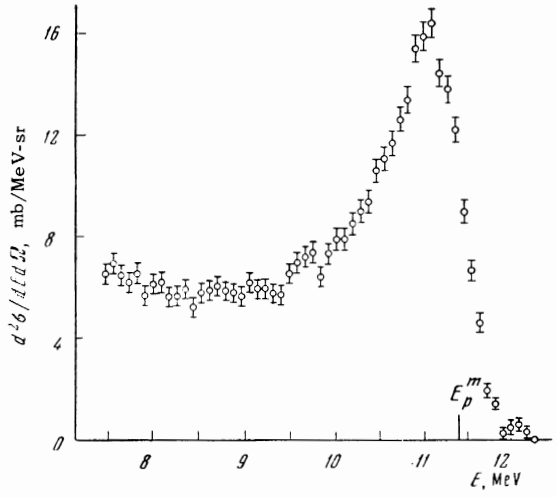

FIG. 4. Energy distribution of 7.5 – 12.0-MeV protons from the reaction D(n,p)2n, emitted at 0° by a 4.3-mg/cm^2 radiator. E_p^m is the theoretical upper limit of proton energy, taking loss in the radiator and the telescope geometry into account.

This background is associated with neutron scattering by hydrogenous impurities and surface films, as well as with n-p reactions either in the parts of the apparatus "seen" by the telescope or in the first scintillation crystal. In the investigated energy region this background did not exceed 5—10% of the main effect. We also subtracted the background of recoil protons resulting from neutron scattering by residual hydrogen in the deuterated polyethylene radiator. A negligible number of random coincidences was observed when a delay was introduced into the coincidence channel circuit.

The channel width for the energy analysis was 90 keV; the statistical accuracy at each point of the curve is 3—5%.

The differential cross section for inelastic scattering was determined most accurately from the intensity ratio between protons emitted in the

investigated reaction and the recoil deuterons for the same radiator:

$$\frac{d^2\sigma}{dE_p d\Omega}(E_p)=\frac{1}{\gamma}\frac{n(E_p)}{n_D}\frac{N_{MD}}{N_{Mp}}\frac{1}{\Omega_0}\int\frac{d\sigma_D}{d\Omega}(\vartheta)f(\vartheta)d\Omega, \quad (13)$$

where $n(E_p)$ is the intensity of protons having the energy E_p in a given analyzer channel, n_D is the intensity of recoil deuterons, N_{MD} is the number of monitor counts in the measurements of deuteron intensity, N_{Mp} is the number of monitor counts in the measurement of the proton energy distribution, γ is the energy channel width in the energy analysis; $\Omega_0 = (\pi\alpha_1\alpha_2)^2$, $\alpha_1 = r_1/d_1$ and $\alpha_2 = r_2/d_2$ are the geometric parameters of the spectrometer (Fig. 5); $d\sigma_D/d\Omega\ (\nu)$ is the cross section for elastic neutron scattering by deuterium when a recoil deuteron is emitted at the angle ϑ relative to the neutron flux direction, $d\sigma_D/d\Omega\ (\nu)f(\vartheta)d\Omega$ is the distribution function of registered recoil deuterons over the angles ϑ. In $n(E_p)$ and n_D experimentally determined corrections were introduced for the counting loss ($\sim 5\%$) resulting from the dead time of the analyzer.

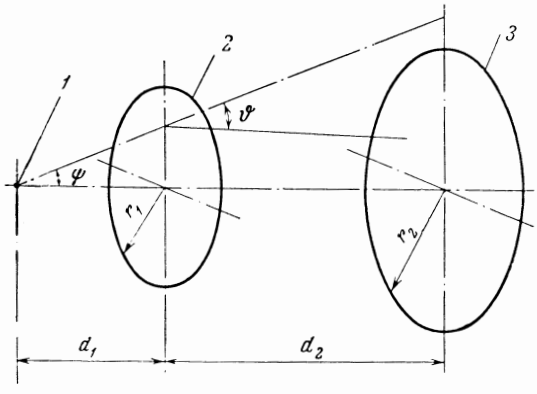

FIG. 5. Spectrometer geometry. 1 – neutron source, 2 – radiator, 3 – particle detector.

Values of $d\sigma_D/d\Omega\ (\vartheta)$ (with 2% accuracy) were taken from [22]. The angular distribution $d\sigma_D/d\Omega\ (\vartheta)f(\vartheta)d\Omega$ was obtained in [23], and was computed on the M-20 electronic computer for the telescope parameters.

The cross section at the peak of the experimental spectrum is 16 mb/MeV-sr; the accuracy of the absolute value of the differential cross section is ±4%.

4. DETERMINATION OF THE CONSTANT ϵ_{nn}

For the purpose of comparison with the experimental spectrum in Fig. 4 the calculated proton energy distributions must take into account the finite parameters of the experimental apparatus (the geometric parameters of the telescope, the radiator thickness, and the resolution of the scintillation counters). The spectral deformation resulting from these factors can be reduced to a nonlinear energy shift and the transformation

$$\frac{d^2\sigma}{dE_p d\Omega_p}(E_p)=\int\psi(E_p,E_1)\frac{d^2\sigma}{dE_1 d\Omega_p}dE_1. \quad (14)$$

To represent (14) exactly, in the calculated spectra, as the resolution function $\psi(E_p, E_1)$ of the spectrometer, we used a matrix for 450 values of each variable. This matrix was based on the experimentally determined shape of the pulse height distribution for recoil protons produced when neutrons were scattered by hydrogen in the polyethylene radiator.

The energy shift of the calculated spectra was determined from the energy distributions of particles registered by the telescope [5)] that were given in [23]. These distributions of protons produced in the reaction D(n, p)2n, emitted at different angles but having identical c.m. energy, were calculated numerically for the geometric parameters α_1, α_2, and $\beta = d_1/d_2$ (Fig. 5) of the given spectrometer and for a selected angle $\chi_0 = 102°$ of neutron emission relative to the deuteron beam direction in the neutron generator. The distributions are shown in Fig. 6 for one of the proton energies in the c.m. (maximum) function.

The distributions of $d^2\sigma/dE_p d\Omega_p$ calculated as functions of E_p, containing ϵ_{nn} as a parameter, were normalized to the experimental spectrum in the interval 10.2–10.6 MeV. For the comparison of the calculated curves with the experimental spectrum the energy scale was refined by introducing a shift δ which was a linear function of the energy and was varied in steps of 9 keV at E_p^m. The constant D′ for each value of ϵ_{nn} and δ was determined from the normalization conditions calculated by least squares. In the region of the peak the part represented by D′ contributes $\approx 30\%$ to the total amplitude.

Figure 7 shows the calculated curves, normalized to the experimental spectrum, corresponding to several values of ϵ_{nn} and the optimum shift δ. The sensitivity of curve shape to ϵ_{nn} decreased compared with (2) (converted to the lab. system) because of the finite spectrometer resolution.

[5)] In [23] distributions of the registered particles were obtained with respect to angles and energies (for the elastic scattering of neutrons by hydrogen and their inelastic scattering by deuterium) for a telescope with a thin radiator.

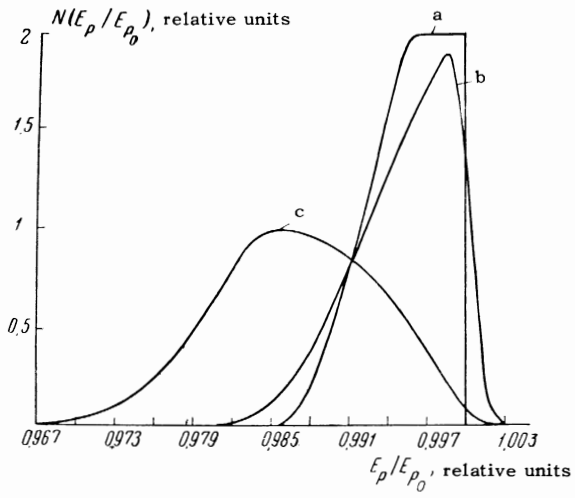

FIG. 6. The function $N(E_p/E_{p_0})d(E_p/E_{p_0})$, which is the distribution of protons registered by the telescope after being emitted when neutrons were scattered inelastically by deuterium. E_p - proton energy; E_{p_0} – energy of a proton emitted at 0° (both in the lab system). a – $N_1(E_p/E_{p_0})d(E_p/E_{p_0})$, the distribution for an infinitely thin radiator when the neutron energy spread is neglected; b – $N_2(E_p/E_{p_0})d(E_p/E_{p_0})$, the distribution for nonmonoenergetic protons; c – $N_3(E_p/E_{p_0})d(E_p/E_{p_0})$, the distribution for a radiator of finite thickness.

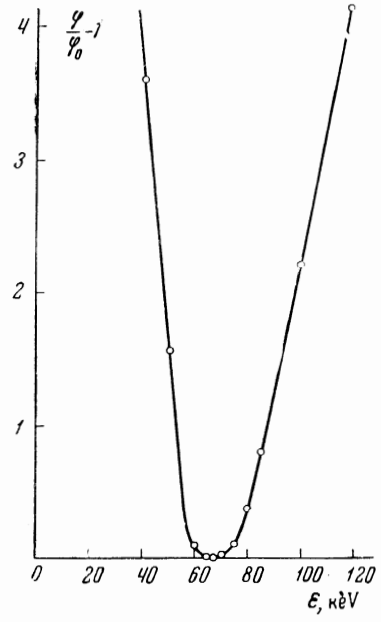

FIG. 8. Graph of $F(\epsilon_{nn}) = \varphi(\epsilon_{nn}) / \varphi_0 - 1$.

The most likely value of ϵ_{nn} was also determined by least squares. The calculated and experimental differential cross sections were compared for 10.2—12.0-MeV protons, for which the energy of relative neutron motion is $E_{nn} < 1$ MeV.

Figure 8 is a graph of $F(\epsilon_{nn}) = \varphi(\epsilon_{nn})/\varphi_0 - 1$, where φ_0 is the sum of least squares for the optimum shift δ, and $\varphi(\epsilon_{nn})$ is the sum of weighted squared deviations. All calculations were performed with the M-20 computer. In estimating the accuracy of the determination of ϵ_{nn} we took into account errors associated with approximations used in deriving the theoretical dependence of $d^2\sigma_0/dE_p d\Omega_p$ on E_p, errors in determining the absolute magnitude of the cross section and constant D′, statistical errors in measuring the spectrum within the region of comparison, small errors associated with the influence of previously scattered neutrons, and inaccuracy in determining the energy scale and resolution function of the spectrometer.

In estimating the accuracy the curve shape was characterized by the value of the differential cross section normalized to the experimental spectrum in the region of comparison, and the dependence $\epsilon_{nn} = f(d^2\sigma/dE_p d\Omega_p, E_p)$ averaged over this energy region was employed.

If the calculated spectra are compared only with experimental values $E_{nn} < 1$ MeV the theoretical approximations can lead to errors of +15% or −11% in the value of ϵ_{nn}. The inaccuracy of D′ and of the absolute magnitude of the cross section can lead to errors of +8% or −6% in ϵ_{nn}. For the curve exhibiting the best agreement we have $\epsilon_{nn} = 67^{+12}_{-9}$ keV (with the rms errors) or $a_{nn} = -23.6^{-1.6}_{+2}$ F.

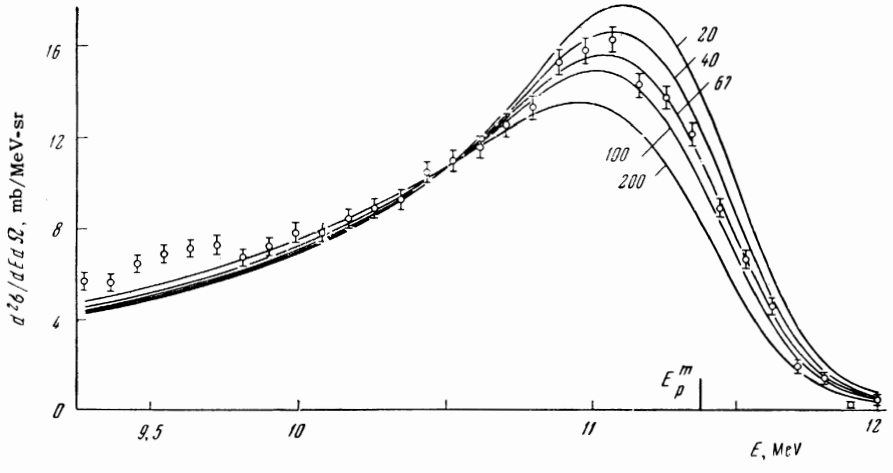

FIG. 7. Calculated differential cross sections for inelastic neutron scattering by deuterium (taking into account the finite parameters of the experimental apparatus), normalized to the experimental spectrum.

5. DISCUSSION OF RESULTS

Figure 9 shows the theoretical proton distribution normalized to the experimental spectrum [without the transformation (14)] in the c.m. system for ϵ_{nn} = 67 keV with $f^2/k_0^{\prime 2} \ll 1$. The differential cross section at the maximum is 20.7 mb/MeV-sr in the c.m. system and 32.8 mb/MeV-sr in the lab. system. The experimental results exclude the possibility of a bound state of two neutrons. The calculated curve for a bound state with ϵ_{nn} = 70 keV, normalized to the experimental spectrum for ~ 10-MeV protons,[6] is shown in Fig. 10. Because of the finite spectrometer resolution a monochromatic line that is located $\frac{2}{3}\epsilon$ (c.m.s) from the upper limit of the continuous spectrum is superimposed on the continuous proton distribution.

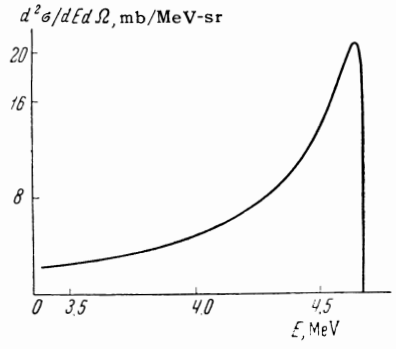

FIG. 9. Theoretical differential cross section for the reaction D(n,p)2n, normalized to the experimental spectrum, for ϵ_{nn} = 67 keV (c.m.s.) with $f^2/k_0'^2 \ll 1$.

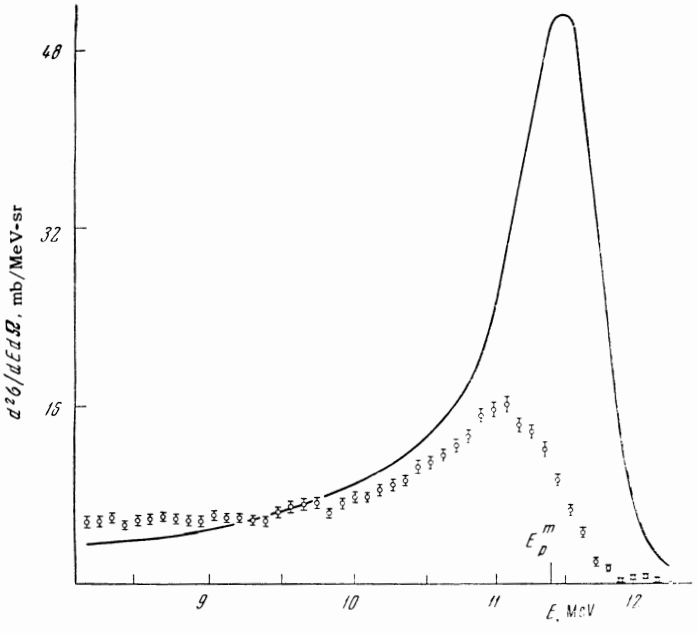

FIG. 10. Theoretical differential cross section for the reaction D(n,p)2n, normalized to the experimental spectrum (allowing for finite instrumental parameters), for a bound state with ϵ_{nn} = 70 keV. The experimental points are shown along with a curve representing the theoretical cross section.

A comparison of our value $a_{nn} = -23.6^{-1}_{+2}{}^{\cdot 6}$ F with $a_s^{np} = -23.74 \pm 0.09$ F [1] shows that charge independence is fulfilled in the S state. The experimental value of a_{nn} is close to the value -27 ± 1.4 F predicted by Wong and Noyes [24] for strict charge symmetry.

The authors are indebted to A. B. Migdal, K. A. Ter-Martirosyan, I. S. Shapiro, V. N. Gribov, P. E. Spivak, G. S. Danilov, V. V. Komarov, and A. M. Popova for discussions and useful suggestions; to A. B. Gil'varg, A. I. Novikov, R. S. Silakov, A. A. Sirotkin, and G. V. Spiridonov for experimental assistance; to A. A. Rodionova for assistance with the calculations performed on the M-20 computer.

[1] MacGregor, Moravcsik, and Stapp, Ann. Rev. Nuclear Sci. 10, 291 (1960).

[2] A. B. Migdal, JETP 28, 3 (1955), Soviet Phys. JETP 1, 2 (1955).

[3] K. M. Watson, Phys. Rev. 88, 1163 (1952).

[4] Panofsky, Aamodt, and Hadley, Phys. Rev. 81, 565 (1951).

[5] R. H. Phillips and K. M. Crowe, Phys. Rev. 96, 484 (1954).

[6] G. V. Skornyakov and K. A. Ter-Martirosyan, JETP 31, 775 (1956), Soviet Phys. JETP 4, 775 (1957).

[7] G. S. Danilov, JETP 40, 498 (1961), Soviet Phys. 13, 349 (1961).

[8] G. S. Danilov, JETP 43, 1424 (1962), Soviet Phys. JETP 16, 1010 (1963).

[9] G. S. Danilov and V. I. Lebedev, JETP 44, 1509 (1963), Soviet Phys. JETP 17, 1015 (1963).

[10] R. D. Amado, Phys. Rev. Letters 2, 399 (1959).

[11] I. S. Shapiro, JETP 41, 1616 (1961), Soviet Phys. JETP 14, 1148 (1962).

[12] I. S. Shapiro, Teoriya pryamykh yadernykh reaktsiĭ (The Theory of Direct Nuclear Reactions), Gosatomizdat, 1963.

[13] V. V. Komarov and A. M. Popova, JETP 45, 214 (1963), Soviet Phys. JETP 18, 151 (1964).

[6] In an approximation in which only pole diagrams contribute to the amplitude and which depends on the f part of the square diagrams in the primary interaction, the calculated cross sections for proton production in the continuous spectrum for real and virtual dineutron levels differ by a factor of several times unity.

[14] G. F. Chew and F. E. Low, Phys. Rev. **113**, 1640 (1959).
[15] Blokhintsev, Dolinskiĭ, and Popov, JETP **42**, 1636 (1962), Soviet Phys. JETP **15**, 1136 (1962).
[16] V. N. Gribov, Nuclear Phys. **5**, 633 (1958).
[17] V. N. Gribov, JETP **41**, 1221 (1961), Soviet Phys. JETP **14**, 871 (1962).
[18] Ilakovać, Kuo, Petravić, Šlaus, and Tomaš, Phys. Rev. Letters **6**, 356 (1961).
[19] Voĭtovetskiĭ, Korsunskiĭ, and Pazhin, PTÉ, in press, 1965.
[20] L. D. Landau, J. Phys. USSR **8**, 201 (1944).
[21] B. B. Rossi, High-Energy Particles, Prentice-Hall, New York, 1952. (Russian translation, Gostekhizdat, 1955, p. 49).
[22] J. D. Seagrave, Phys. Rev. **97**, 757 (1955).
[23] Voĭtovetskiĭ, Korsunskiĭ, and Pazhin, PTÉ, in press, 1965.
[24] D. Y. Wong and H. P. Noyes, Phys. Rev. **126**, 1866 (1962).

Translated by I. Emin
230